Turbulence Modeling of Cavitating Flows in Liquid Rocket Turbopumps

Mani, K.V.; Cervone, Angelo; Hickey, J.P.

DOI
10.1115/1.4034096

Publication date
2017

Document Version
Accepted author manuscript

Published in
Journal of Fluids Engineering

Turbulence modelling of cavitating flows in liquid rocket turbopumps

Karthik V. Mani
German Aerospace Center (DLR)
Spacecraft Department
Bunsenstr. 10, 37073, Göttingen, DE
and
Delft University of Technology
Space Systems Engineering
Kluyverw. 1,2629, Delft, NL
Email: karthikvenkateshmani@gmail.com

Angelo Cervone
Delft University of Technology
Space Systems Engineering
Kluyverw. 1, 2629, Delft, NL
Email: a.cervone@tudelft.nl

Jean-Pierre Hickey*
German Aerospace Center (DLR)
Spacecraft Department
Bunsenstr. 10, 37073, Göttingen, DE
and
University of Waterloo
Department of Mechanical and Mechatronics Engineering
University Ave. 200, N2L 3G1, Waterloo, CA
Email: jean-pierre.hickey@uwaterloo.ca

ABSTRACT

An accurate prediction of the performance characteristics of cavitating cryogenic turbopump inducers is essential for an increased reliance on numerical simulations in the early turbopump design stages of liquid rocket engines. This work focuses on the sensitivities related to the choice of turbulence models on the cavitation prediction in flow setups relevant to cryogenic turbopump inducers. To isolate the influence of the turbulence closure models for Reynolds-averaged Navier-Stokes equations, four canonical problems are abstracted and studied individually to separately consider cavitation occurring in flows with a bluff body pressure drop, adverse pressure gradient, blade passage contraction and rotation. The choice of turbulence model plays a significant role in the prediction of the phase-distribution in the flow. It was found that the sensitivity to the closure model depends on the choice of cavitation model itself; the barotropic-based cavitation models are far more sensitive to the turbulence closure than the transport-based models. The sensitivity of the turbulence model is also strongly dependent on the type of flow. For bounded cavitation flows (blade passage), stark variations in the cavitation topology are observed based on the selection of the turbulence model. For unbounded problems, the spread in the results due to the choice of turbulence models is similar to non-cavitating, single-phase flow cases. A set of considerations for turbopump designers are provided for an informed decision on the selection of turbulence models.

*Corresponding author

Nomenclature

σ Cavitation number
P Pressure
p_∞ Freestream pressure
p_{sat} Saturation pressure at defined temperature
m,v,l Mixture, vapour, liquid state
ρ Density
T Temperature
U Velocity
U_∞ Free stream velocity
$C_{p_{min}}$ Coefficient of Pressure at minimum pressure
a Speed of sound
ν Kinematic viscosity
μ Dynamic viscosity
ψ Compressibility
t Time
μ_t Turbulent eddy viscosity
α Volume fraction
γ Vapour phase fraction
$\dot{m}^+$ Condensation source term
$\dot{m}^-$ Evaporation source term
k Turbulent kinetic energy
ε Dissipation rate of the turbulent kinetic energy
ω Specific dissipation rate of the turbulent kinetic energy
$C_{\varepsilon 2}$ Constant in the dissipation rate equation

1 Introduction

Turbopumps in liquid rocket engines (LRE) deliver propellants, such as liquid hydrogen (LH2) and liquid oxygen (LO2), from low pressure storage tanks to a high pressure combustion chamber [1]. They are a central component in LREs as they control both injection pressure and propellant mass flow rate to the combustor. The design and analysis of turbopumps is highly complex due to high rotational speeds, and potential for the onset of vibrations and flow instabilities while simultaneously needing to meet the stringent performance and weight requirements of the system [1, 2].

The mass and size constraints imposed to the turbopump means that a high rotational speed (often over 20,000 rpm) is needed in order to deliver the required mass flow rate of propellants to the combustor. Because of the high rotational speeds, cavitation is likely to arise on the suction side of the blade passages as the static pressure of the liquid drops down to its vapour pressure [1]. Cavitation is to be avoided as it leads to a reduction of the pump efficiency, mixing losses, erratic mass flow rate, insufficient power to the fluid, and can result in dangerous vibrations and instabilities. In a turbopump assembly, an axial impeller called *inducer* is placed in front of the main impeller on the same shaft with the same rotational speed [1]. The inducer marginally increases the liquid pressure such that cavitation is avoided or severely reduced at the main impeller inlet. These inducers are designed to operate at controlled cavitating conditions to improve overall pumping performance of the turbopump assembly.

The onset and extent of cavitation arising in the inducer is a key parameter in the design of the turbopump assembly. Ideally, the cavitation characteristics should be assessed early in the design stages. This forces the turbopump designer to heavily rely on empirical correlations and fits for an *apriori* estimate of cavitating characteristics. Naturally, experimental methods are the most robust and accurate means of obtaining cavitation onset, extent, and topology. Several academic works have investigated the cavitating characteristics of inducers, including: Stripling and Acosta [3], Cervone *et al.* [4–7], and Tsujimoto *et al.* [8, 9]. Experiments have the greatest fidelity but they are inherently iterative, time consuming, and expensive. Numerical modelling of cavitating inducers provides a useful complement to empirical methods and experiments that is inexpensive, rapid and can be

integrated early in the design phase of the turbopump assembly. Furthermore, numerical tools can be coupled to optimization algorithms for improved design convergence. But, numerical modelling generally lacks predictive capability. At present, there is a large amount of modelling uncertainty associated with the numerical simulations of cryogenic cavitating flows, especially in regards to the cavitation, thermal effects and turbulence modelling. In the present work, we report on the influence of turbulence modelling on cavitating cryogenic inducer flows.

The cavitating turbulent flows can be simulated–without resorting to any modelling approximations–by directly solving the conservation equations (mass, momentum and energy) for all phases, at all temporal and spatial scales of turbulence of the problem. Direct Numerical Simulation (DNS) of cavitating flows has been undertaken (e.g. [10]) for problems with a reduced scale-separation (e.g. micro-channel cavitation). Under a number of simplifying approximation, based on the assumed isotropy of the small-scale turbulence, Large Eddy Simulation (LES) can also be used to account for the turbulence, at a more affordable computational cost [11, 12]. Owing to very high rotational speeds and correspondingly large Reynolds numbers ($6 - 22 \times 10^6$) associated with turbopump inducer flows, DNS and LES become impractical in a fast-paced industrial context [11, 13]. In the Reynolds-averaging approach (RANS), the time-averaged Reynolds stress terms are modelled using a number of different modelling approximations. Because RANS-based approaches are computationally advantageous, they remain the standard tool for turbulence modelling in cavitating turbopump flows in most applied settings. The RANS closure models have been historically constructed to accurately capture the essential characteristics of single phase, canonical flows (*e.g.* boundary layer, backward facing step, wake, jet). The robustness of RANS has lead to these closure models being used for flow in which the original modelling assumptions no longer hold. For cavitating flows, and particularly in the turbopump CFD community, the prevailing assumption is that the cavitation modelling is of primary importance; thus, the turbulence modelling of cavitating RANS simulations is often overlooked. In this work, we seek to challenge this assumption and quantify the relative importance of the turbulence modelling for cavitating cryogenic flows in LRE inducers.

A limited number of works have addressed the RANS turbulence closure for cavitating flow simulations. Goncalves [14] presents a one-fluid compressible, RANS solver with a stiffened gas equation of state for the mixture and assesses the turbulence modelling influence in canonical cavitating flows. Decaix *et al.* [15, 16] developed and compared RANS-based correction models for unsteady cavitating flow simulations. Wu *et al.* [17, 18] assess the modelling strategies for turbulent cavitating flows by using $k-\varepsilon$ turbulence model with Launder-Spalding description and filter-based methods. Higher-order closure models have also been addressed. Mashayek *et al.* [19] provide a description of second-moment closure approaches for two-phase flows. Cokljat *et al.* [20] and Beishuizen *et al.* [21] discuss the Reynolds stress models for Eulerian multiphase flows and turbulent dispersed two-phase flows respectively. To the knowledge of the authors, and after a wide literature survey, no work has specifically addressed the uncertainty associated with the choice of turbulence models on cavitation predictions in multiple flow regimes found in cryogenic turbopump inducers. Thus, the objectives of this work are: (a) To address the uncertainty associated with the choice of turbulence models in cryogenic turbopump inducer cavitating flow simulations; (b) To transpose the knowledge gained to turbopump designers in order to assist them in their choice of modelling assumptions.

In the following section, a description of the numerical methods and a listing of the abstracted test cases are presented. The sensitivity of the turbulence models are analyzed in section 3. Finally, a discussion of the take-away results for the turbopump designer is presented in section 4.

2 Computational modelling and setup

2.1 Numerical tools

The numerical simulations were conducted using the open-source CFD package: OpenFoam, version 2.2 [22]. Two separate cavitation solvers were used in order to comparatively quantify the sensitivity of the choice of cavitation model. The cavitation solvers solve the conservative form of the Navier-Stokes equation but use different approaches in handling the state equation and the two-phase modelling. The first solver is based on a barotropic equation of state (denoted herein as BES - Barotropic Equation-of-state based Solver), which directly couples the density to the pressure [23, 24]. The minimal speed of sound of the mixture is used as a fitting parameter for the model.

$$\frac{D\rho}{Dt} = \psi \frac{DP}{Dt} \tag{1}$$

$$\psi = \frac{1}{a^2} \tag{2}$$

$$\rho_m = (1-\gamma)\rho_l + (\gamma\psi_v + (1-\gamma)\psi_l)P_{sat} + \psi_m(P - P_{sat}) \tag{3}$$

$$\psi_m = \gamma\psi_v + (1-\gamma)\psi_l \tag{4}$$

where ρ is the density, P is the pressure, ψ is the compressibility expressed as a reciprocal of speed of sound (a) squared and γ is the vapour phase fraction ($\gamma = 1$ denotes pure vapour phase). The subscripts m, l, v, and sat denote mixture, liquid, vapour, and saturation quantities respectively.

The second solver is based on a supplementary transport equation for the liquid volume mass fraction α_l void (TES - Transport Equation based Solver). The volume fraction is used to reconstruct the mixture density based on the respective densities of the liquid and gas phases. The liquid volume fraction transport equation and the mixture density are expressed as,

$$\frac{\partial \alpha_l}{\partial t} = \frac{\partial}{\partial x_j}(\alpha_l u_i) = \dot{m}^+ + \dot{m}^- \tag{5}$$

$$\rho_m = \alpha_l \rho_l + (1-\alpha_l)\rho_v \tag{6}$$

The transport equation contains a source ($\dot{m}^+$) and a sink ($\dot{m}^-$) term to account for cavitation production and destruction; cavitation source and sink terms are modelled based on the formulae proposed by Kunz et al. [25]. The TES is applicable for two incompressible, isothermal immiscible fluids with phase change that incorporates the Volume of Fluid (VoF) phase fraction based interface capturing methods. This solver allows for the modelling of the impact of inertial forces on cavities such as elongation, detachment, and drift of bubbles [26].

A number of turbulence closure models were used for this investigation. All models correspond to the classic implementation with standard coefficients (see [27] or [28] for a summary of the models). The turbulence closure models used are highlighted in section 3.

2.2 Numerical methods and schemes

The interpolation from cell centers to face centers is done using a linear interpolation scheme. The convection terms used are computed by Gaussian integration which, combined with the linear interpolation, results in a second-order spatial accuracy. The Laplacian terms in the conservative Navier-Stokes equation, for example $\nabla \cdot (\nu \nabla U)$, use Gaussian integration for discretisation, a second-order linear interpolation scheme, and uses an explicit non-orthogonal correction which is second-order, bounded and conservative for surface normal gradient calculation. Implicit Euler scheme is used for temporal discretisation which is of first-order and is bounded.

2.3 Case description

To systematically analyse the influence of the turbulence model on the cavitation prediction, the turbopump is abstracted and the various flow regimes are isolated. Addressing the turbulence modelling influence in a realistic configuration is far too complex because of the strong mutually coupled interactions, the lack of detailed experimental data and computational cost associated to such simulations. Simplification and abstraction of the problems increases the computational feasibility, allows a clearer interpretation of the causes of cavitation prediction variation, and eliminates uncertain behaviour due to unknown coupling effects. Furthermore, well-established test cases provide trustworthy experimental data. In the present work, the cavitating turbopump cavitation was

divided into four separate sub-problems which correspond to: bluff body cavitation, internal blade passage cavitation (suction side), attached leading edge cavitation with a pressure gradient, and cavitation in a rotational frame of reference. Figure 1 illustrates the investigated regimes and their corresponding location in the inducer. The computational domains and setups (for the simple test cases) are fully defined in the figure.

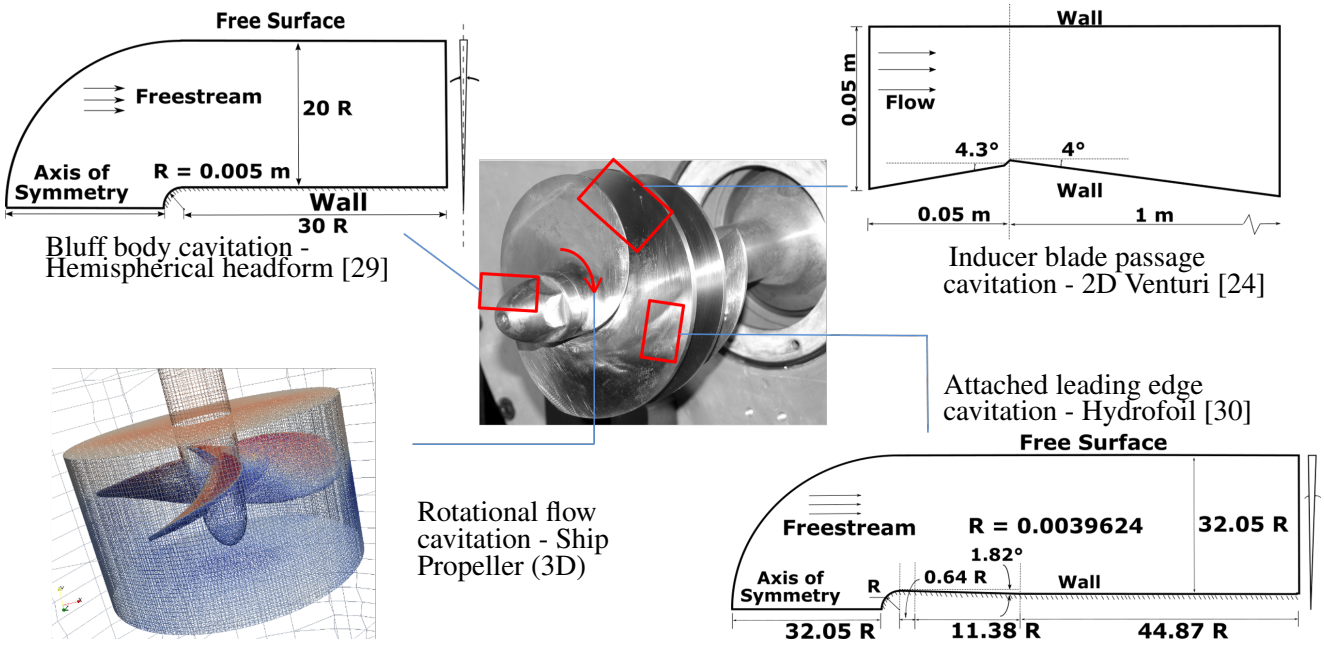

Fig. 1: Simplification of a 3D inducer geometry into canonical flow problems: (top left) bluff body cavitation at the inducer boss - hemispherical headform [29], (top right) attached leading edge cavitation - hydrofoil [30], (bottom right) inducer blade passage cavitation - 2D Venturi [24], (bottom left) rotational flow cavitation - 3D rotating ship propeller.

The first case deals with the bluff body cavitation occurring at the inducer boss. This domain is simplified to an axisymmetric hemispherical headform. This problem corresponds to the setup investigated by Rouse and McNown (1948) [29]. The second case focuses on attached leading edge cryogenic cavitation, using liquid hydrogen at 20 K past an axisymmetric hydrofoil with a positive pressure gradient downstream of the flow [30]. It should be noted that the thermal effects resulting from evaporative cooling are not included in our cavitation models. The third case abstracts the cavitation occurring in the inducer blade passage as a 2D Venturi [24]. The final case deals with the effect of rotation on cavitation investigated by simulating water flow past a rotating ship propeller. Figure 1 summarizes the numerical domains for hemispherical headform, 2D venturi, and hydrofoil cases.

2.4 Case details and boundary conditions

To investigate the effect of turbulence models, baseline configurations for each of the aforementioned cases are established with a fixed set of simulation parameters. Then, the turbulence models are varied and the cavitation predictions are quantified and analysed. The baseline simulation parameters are listed in table 1.

In the descriptions of baseline configurations, solid boundaries such as the headform, hydrofoil, the Venturi tube, and the propeller blades are treated as no-slip walls. Standard wall functions are applied for the first three cases and rotating wall functions are applied in the last case. Standard wall functions correspond to law of the wall, in which the near wall velocity has a logarithmic variation in the normal direction [31]. The hemispherical headform and hydrofoil domains are designed as a wedge plane to emulate a 2D axisymmetric domain. The Venturi is configured as a 2D domain while the propeller is a 3D rotating domain. The inflow boundary conditions prescribed the density, temperature, and velocity, of the pure liquid phase; the pressure is fixed at the outflow boundaries at the freestream value.

2.5 Grid details and convergence

An optimized, fully-structured mesh was used for all two-dimensional cases. A convergence study was undertaken for the cases to assure the grid independence of the results. The y^+ value at the wall and total grid points for the regular mesh in all cases are indicated in table 1. For sake of conciseness, the grid convergence results are only shown for the hydrofoil case with positive pressure gradient [30]. Figure 2a shows the time-averaged density field for the coarse, regular and fine mesh. The regular mesh is made up of 5.52E5 grid points which are clustered near the non-slip walls. The coarse and fine mesh respectively divide and multiply by two the number of grid points in each direction (1.37E5 and 2.2E6 grid points). Various quantities were analysed to assure convergence such as the pressure distribution (C_p) along the hydrofoil and wall normal velocity, density, pressure and turbulence intensity profiles. Figure 2a shows the cavitation bubble topology and figure 2b shows the quantitative comparison of the wall-normal density and pressure profile among the various grid resolutions. We assured that the integral cavitation length remained invariant to the grid refinement as the basis for the selection of the appropriate grid.

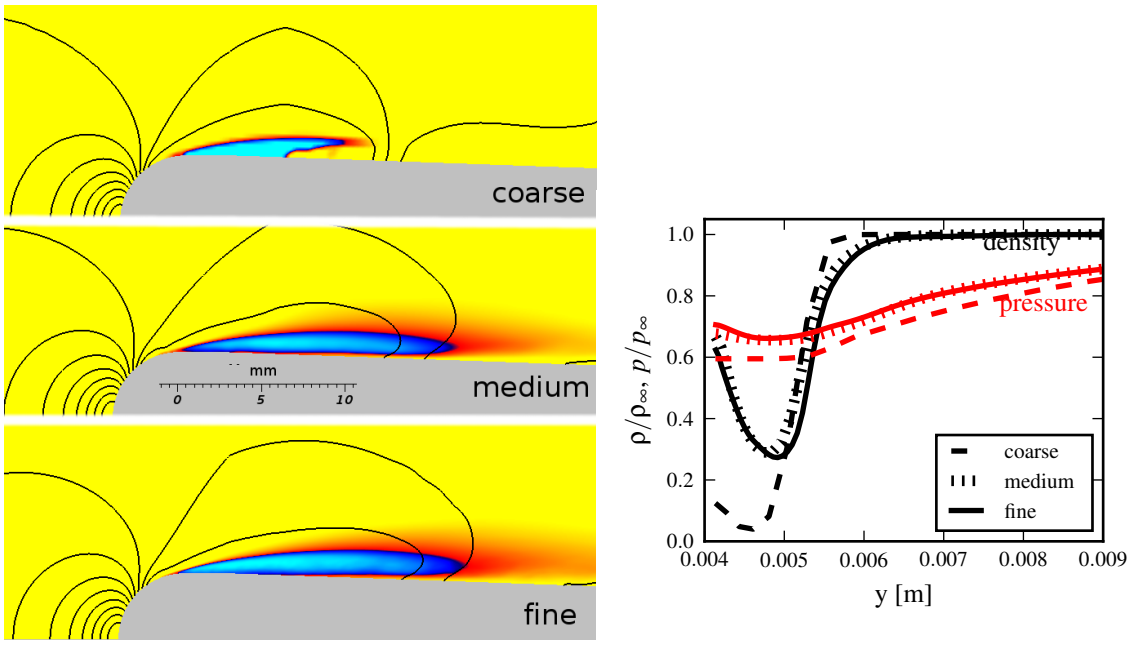

(a) cavitation topology

(b) normalized pressure and density at x=5 mm

Fig. 2: Grid convergence study of the hydrofoil. (a) contour plot showing time-averaged pressure (lines) and density (color); (b) quantitative comparison of normalized pressure and density at x=5 mm.

3 Influence of turbulence models

The investigated cases use $k-\omega$ SST as the baseline turbulence model. To test the influence of the turbulence modelling, four other models are investigated, namely: $k-\varepsilon$, RNG $k-\varepsilon$, $k-\omega$, and Launder-Reece-Rodi Reynolds Stress Model (RSM - LRR). Reynolds averaging of the Navier Stokes equations produces a Reynolds stress tensor which requires closure. The Reynolds stresses have 6 components (assuming symmetry of the off-diagonal terms) which, for modellign purposes, are then represented in terms of the time-averaged velocity components. The Boussinesq hypothesis is used to simplify the Reynolds stress tensor and expresses it as a sum of isotropic and anisotropic parts [11]. The former contains the turbulent kinetic energy and the latter contains the energy dissipation rate. All models used, except for the RSM, are considered to be two equation turbulence closure models, i.e., they require two extra transport equations to provide closure to the problem. The RSM uses a transport equation for each of the six Reynolds stress components and a transport equation for the energy dissipation rate. For conciseness, the details of each of these turbulence models are left out; the reader is invited

Parameters	Hemispherical Headform	Hydrofoil	2D Venturi	Propeller
Fluid	Water	LH2	Freon R-114	Water
Temperature, T_∞ [K]	298	20	293	298
Cavitation Number, σ [-]	0.5	0.35	0.55	0.868
Velocity, U_∞ [m/s]	19.8	53.0	14.4	15
Pressure, p_∞ [Pa]	101325	84329	265300	101325
Density, ρ_l [$\mathrm{kg \cdot m^{-3}}$]	997.05	73.47	1470.6	1000
Turbulence model	$k-\omega$ SST	$k-\omega$ SST	$k-\omega$ SST	$k-\omega$ SST
Mesh resolution, y^+_{wall}	87.5	692	38.5	unstructured
Grid points	5.03E5	5.52E5	6.51E5	6.56E5

Table 1: Baseline simulation parameters

to consult [28] for a summary of these models. In addition, certain cases are simulated without any turbulence (laminar flow) to test the overall importance of turbulence on the mean flow.

3.1 Hemispherical headform - bluff body cavitation

The baseline cases are solved with both the BES (barotropic equation of state) and TES (transport equation solver) approaches. To validate the baseline results, the obtained normalized pressure distributions along the non-dimensionalized surface distance are compared with experimental results [29]. The plots in figure 3 show normalized pressure distributions, $C_p = (p - p_\infty) / \left(0.5\rho_l U_\infty^2\right)$, plotted along the surface distance normalized by the diameter of the hemispherical headform s/d. Here p and p_∞ are the local and freestream pressures, respectively. The minimum C_p for BES and TES are 6.33% lower and 0.588% higher than the literature value ($C_{p,min} = -\sigma = -0.5$) respectively and the attached cavitation length (calculated at the wall) obtained for BES and TES are $0.45d$ and $0.38d$ respectively.

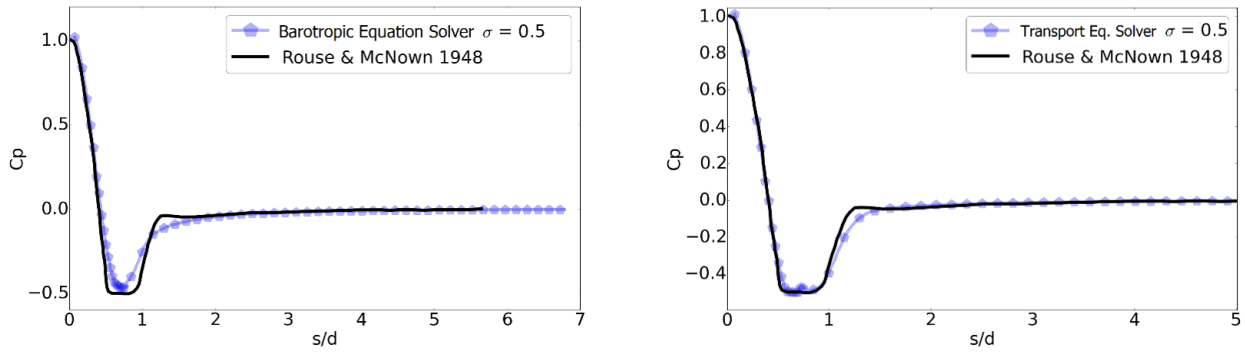

(a) BES (b) TES

Fig. 3: Baseline validation for BES and TES of the hemispherical headform.

The turbulence model is varied and the variations in $C_{p,min}$, cavitation lengths, pressure distribution, density distribution (for BES), and liquid volume fraction distributions are quantified and analysed. Figure 4 shows the normalized pressure (C_p) distribution. In BES simulations, the $k-\varepsilon$ model pressure distribution differs significantly from that of the baseline $k-\omega$ SST. A discontinuous cavity bubble is observed. The density distributions are significantly different for each model but the global cavitation length variation is minor except for RSM and $k-\varepsilon$. The RSM model predicts early cavitation onset and collapse with a 27% reduction in cavitation length. In TES simulations, all turbulence models exhibit similar pressure distributions with maximum deviation being 0.59%. Cavitation bubble size variation is negligible. This indicates that the choice of the solver has a major effect on the turbulence model influence. This finding has significant implications, as the sensitivity of the turbulence model depends on the choice of cavitation solver.

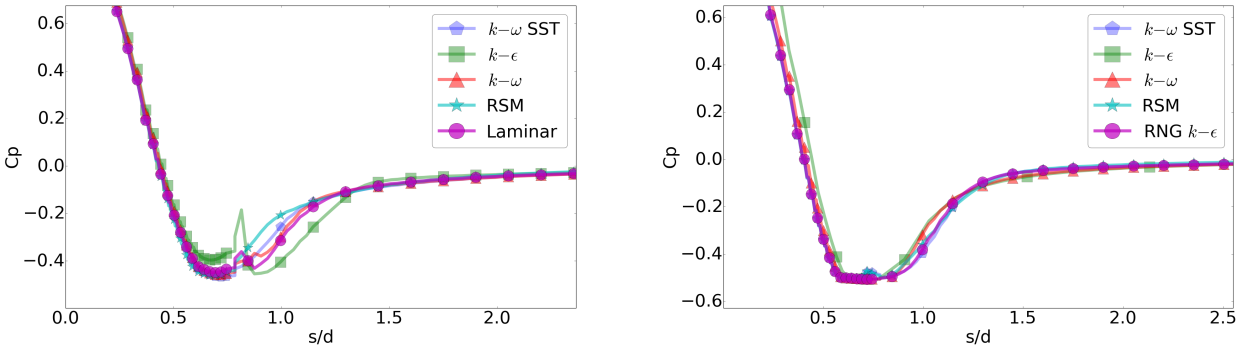

(a) Normalized pressure distribution - BES

(b) Normalized pressure distribution - TES

Fig. 4: Hemispherical headform normalized pressure distributions - turbulence model influence

Case	Cav. Length	Cav. Onset	$C_{p,min}$
$k-\omega$ SST (BES)	0.450 d	0.637 d	-0.468
$k-\omega$ SST (TES)	0.378 d	0.588 d	-0.503
Case	Δ Cav. Length	Δ Cav. Onset	$\Delta C_{p,min}$
	BES		
$k-\varepsilon$	0.130 d (28.88%)	0.021 d (3.30%)	0.014 (-2.99%)
RSM	-0.124 d (-27.55%)	-0.087 d (-13.65%)	0.007 (-1.49%)
	TES		
$k-\varepsilon$	0.028 d (7.40%)	0.036 d (6.12%)	-0.003 (0.59%)
$k-\omega$	0.049 d (12.96%)	0.011 d (1.87%)	-0.002 (0.39%)

Table 2: Hemispherical headform variations in cavitation lengths, onset distances, and $C_{p,min}$ for BES and TES - turbulence model influence. Listed are the significantly varying results.

3.2 Hydrofoil - attached leading edge cavitation

The variation in the pressure coefficient, C_p, for both solvers is shown in figure 5 for the hydrofoil with positive pressure gradient. The transport-based cavitation model shows a negligible variation in $C_{p,min}$, however, the difference in the cavitation length associated with BES is $\sim 0.9d$ larger than that of TES.

In BES simulations, the pressure distributions vary by a large margin, especially for the $k-\omega$ model. It is conjectured that the positive pressure gradient downstream of the hydrofoil forces an early pressure recovery by the $k-\omega$ model due to its sensitivity to adverse pressure gradients (positive or negative) in the flow. The laminar simulation results in a similar pressure recovery, although not as strong. This is expected given the higher sensitivity (due to inflectional instability of the mean flow profile) of the laminar profile to the adverse pressure gradients. The density distributions associated with $k-\omega$ and laminar formulation also show significant differences compared to the baseline. However, the overall cavitation length variation is minor. In TES simulations, the pressure distribution patterns for all turbulence models are similar with very small differences. The liquid volume fraction distributions predicted by the turbulence models show moderate variations.

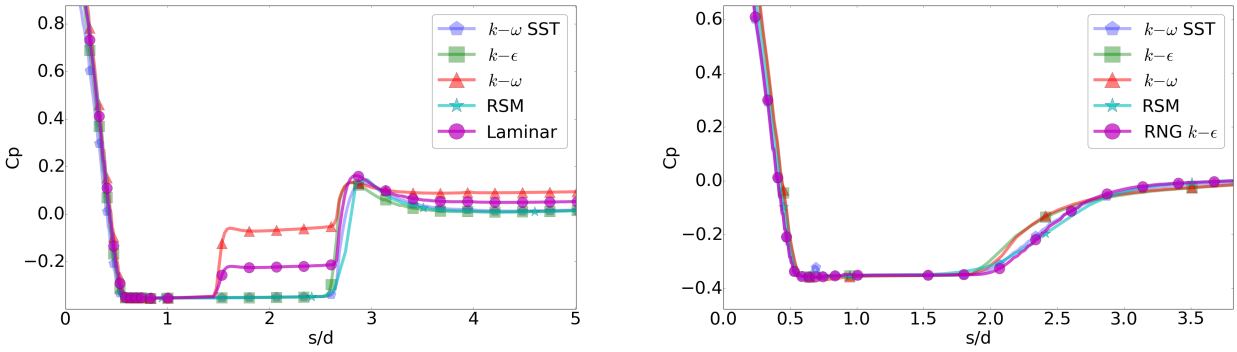

(a) Normalized pressure distribution - BES

(b) Normalized pressure distribution - TES

Fig. 5: Hydrofoil normalized pressure distributions - turbulence model influence

3.3 2D Venturi - Inducer blade passage cavitating flow

The baseline case is setup for TES simulations and most initial parameters are replicated from [24]. Oscillations of the attached cavitation bubble are observed during experiments. However, in the simulations the bubble oscillations are not clearly visible. The primary cause is that the two-equation RANS models tend to over-predict the turbulent viscosity μ_t near the wall which leads to the prevention of the formation of re-entrant jet [23] and thus leading to stable cavities. Reboud [32] proposed an empirical correction term to limit the eddy viscosity, which was not implemented in the present work.

The cavitation length obtained during the baseline simulation is 77.37 mm which lies in the range of 75-80 mm observed during experiments [24], see table 3. The change in turbulence models produced drastic difference in cavitation length and topology (figure 6). The quantity plotted is the instantaneous α_l at a single step. The $k-\varepsilon$ model yields a cavitation length which is 41% larger than that of the $k-\omega$ SST model. The $k-\omega$ however yields 15% less. Although, both $k-\omega$ and $k-\varepsilon$ have similar liquid volume fraction distribution profiles with respect to the $k-\omega$ SST case.

The RSM and RNG $k-\varepsilon$ models yield very high cavitation lengths (increase of 492% and 533% respectively). The RSM behaviour is due to the high sensitivity of the modelled pressure-strain term to the adverse pressure gradients caused by the reflection of pressure from the closely placed walls. Reflection of pressure affects the redistribution of turbulent kinetic energy. The increase of TKE leads to an increase in the magnitude of the wall reflection term which in turn leads to an increase in shear stress parallel to the wall. This elongates the cavity. The slow part of the pressure-strain term is affected by the increase in velocity of the liquid phase caused by the

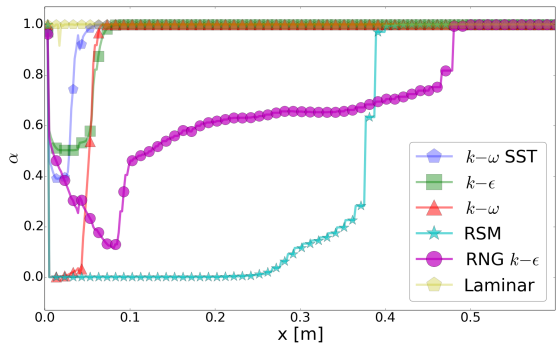

(a) α vs x

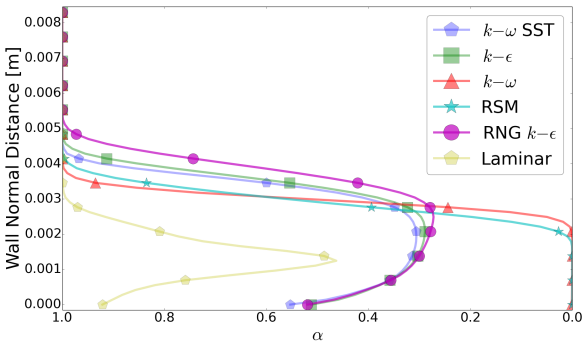

(b) Station 1 : x = 0.014 m

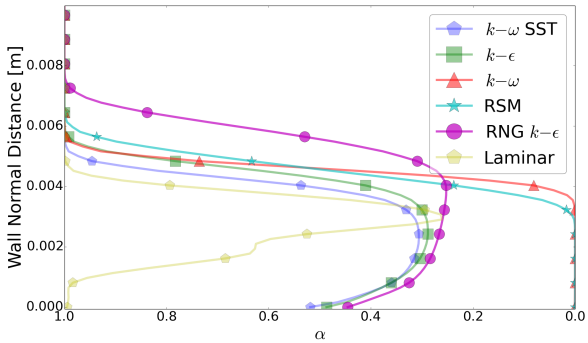

(c) Station 2 : x = 0.024 m

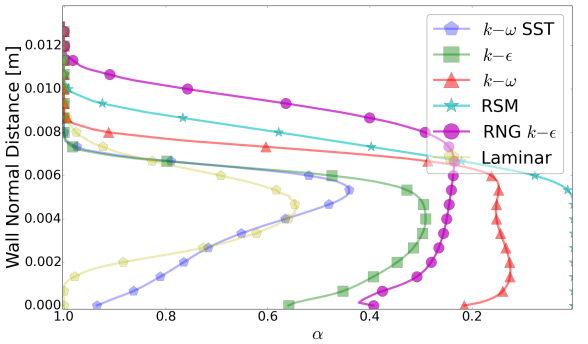

(d) Station 3 : x = 0.048 m

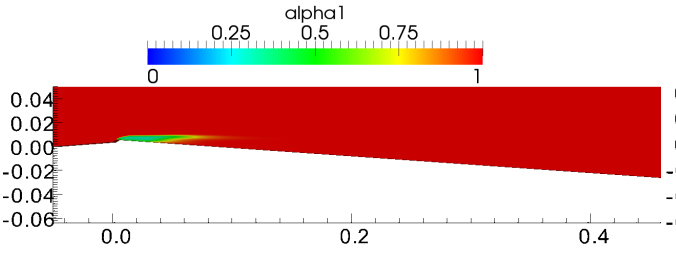

(e) $k-\omega$ SST

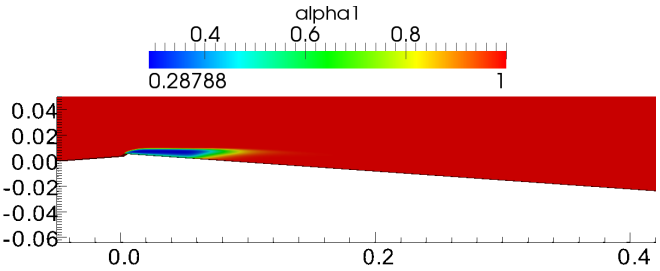

(f) $k-\varepsilon$

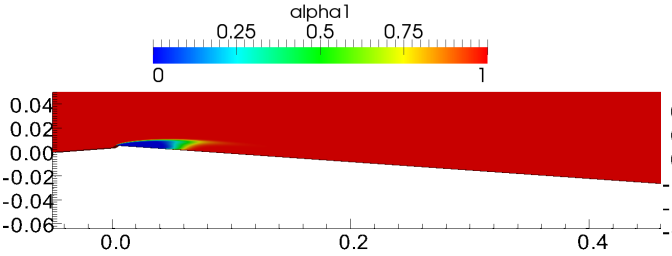

(g) $k-\omega$

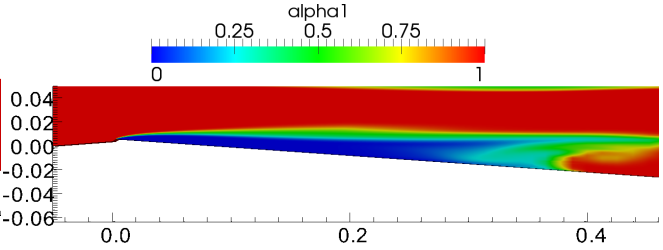

(h) RSM

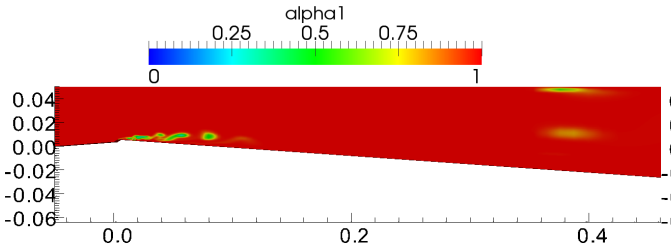

(i) Laminar

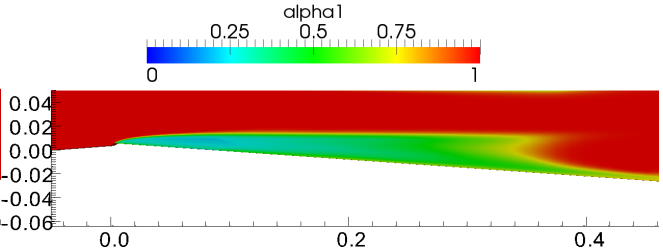

(j) RNG $k-\varepsilon$

Fig. 6: 2D Venturi liquid volume fraction α vs distance x distribution, wall normal α distribution, and contours for $k-\omega$ SST, $k-\varepsilon$, $k-\omega$, RSM, and RNG-$k-\varepsilon$ models

Case	Cavity Length
$k-\omega$ SST	0.077387 m
$k-\varepsilon$	0.109136 m
$k-\omega$	0.065481 m
RSM	0.458370 m
RNG $k-\varepsilon$	0.490118 m

(a) Cavity length

Case	Δ Cav. Length
$k-\varepsilon$	0.031749 m (41.03%)
$k-\omega$	-0.011906 m (-15.38%)
RSM	0.380983 m (492.31%)
RNG $k-\varepsilon$	0.412731 m (533.33%)

(b) Change in cavity length

Table 3: 2D Venturi cavity lengths and their variation for various turbulence models.

restriction in flow, thus leading to further pressure drop and increased stretching of the vapour bubble.

The RNG $k-\varepsilon$ model differs from standard $k-\varepsilon$ formulation by using rigorous mathematical technique [33]. A noticeable difference is the usage of differential turbulent viscosity and a different model constant $C^*_{\varepsilon 2}$ which is lower in magnitude compared to the standard $k-\varepsilon$ constant $C_{\varepsilon 2}$ [11, 33]. This leads to the decrease in production rate of k and dissipation rate ε. This effect reduces the value of μ_t and thereby leads to larger and more unstable cavities.

The laminar simulation does not yield an attached cavitation bubble like the rest of the models. It results in small bubbles generated at the wedge. The distribution of liquid volume fraction in the wall normal direction at three different locations (0.014 m, 0.024 m, 0.048 m) are shown in figures 6b, 6c, and 6d. The variation in the α distribution along the wall normal direction is significant among the turbulence models. The closest result to the corresponding literature [24] is yielded by the $k-\omega$ SST model. This analysis proves that the choice of the turbulence model carries very high importance when numerically simulating inducer flows.

3.4 Propeller - 3D rotating flow cavitation

The 3D rotating flow through a ship propeller is simulated to analyse the effect of rotation on cavitation predictions. Four propeller blades are attached to the main hub and the diameter of the propeller is 0.22 m. It is placed inside a cylindrical casing with diameter and height being 0.24 m and 0.14 m respectively. The fluid used is water.

The turbulence modelling influence on phase distribution is analysed, albeit qualitatively. The inlet velocity of the water is 15 m/s and the rotation rate of the propeller is 53.93 rad/s (515 rpm). The basic fluid properties are listed in table 1. The solver used is the TES with the capability to handle rotating meshes. Thus we analyse the liquid volume fraction contours qualitatively and determine the difference in distributions due to change in turbulence models.

The turbulence models $k-\omega$ SST and $k-\varepsilon$ exhibit similar behaviour. However, a stark difference is observed in the case of $k-\omega$ model. These differences are due to the sensitivities of the models to adverse pressure gradients in the freestream region. The $k-\omega$ SST formulation uses blending functions and uses $k-\omega$ formulation near the wall and $k-\varepsilon$ formulation in the freestream region. $k-\omega$ model is very sensitive to adverse pressure gradients in the freestream whereas $k-\omega$ SST and $k-\varepsilon$ are not. The RNG $k-\varepsilon$ model and RSM exhibit behaviours which differ moderately. RNG $k-\varepsilon$ model has improved predictions for flows with high streamline curvature with some improved accuracy for rotational flows, whereas RSM inherently accounts for rotation and the associated anisotropies.

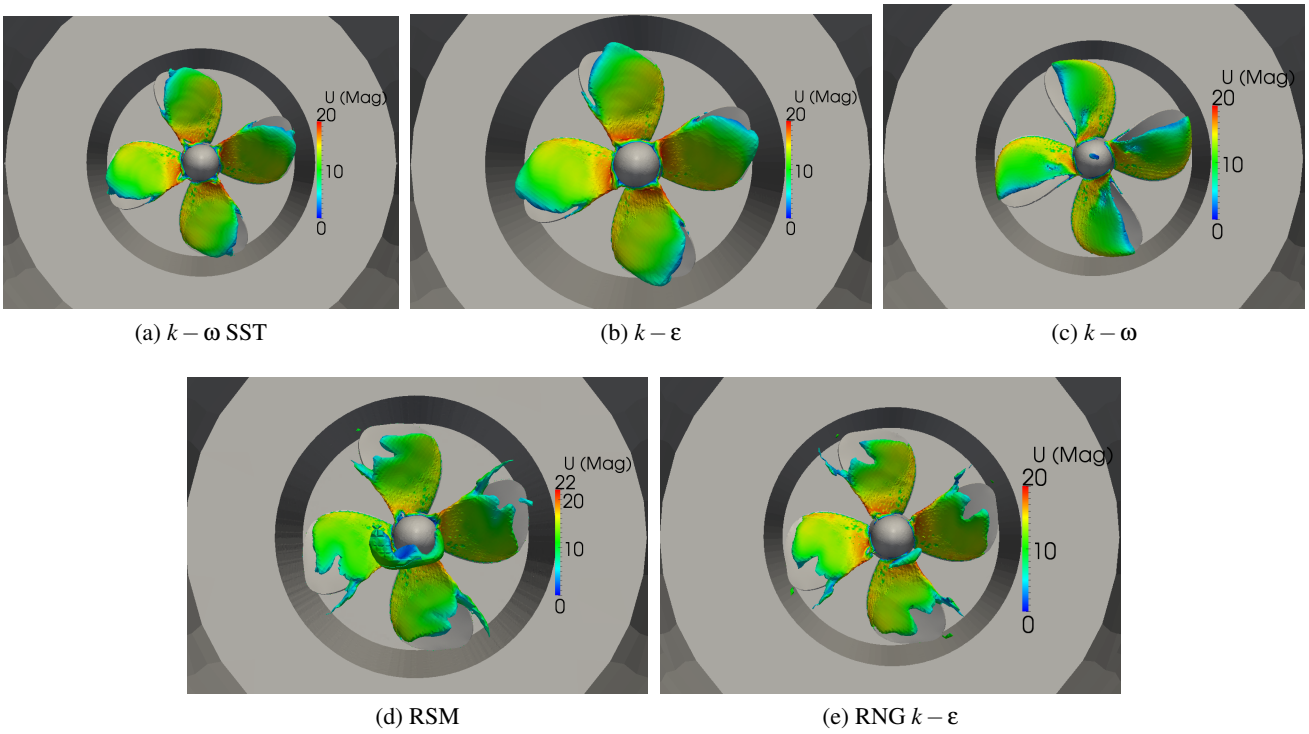

(a) $k-\omega$ SST (b) $k-\varepsilon$ (c) $k-\omega$

(d) RSM (e) RNG $k-\varepsilon$

Fig. 7: Rotating propeller phase distribution contours at $\alpha = 0.5$. The direction of rotation is clockwise. The contours are coloured according to the magnitude of velocity.

4 Discussion and conclusion

Numerical modelling of cavitating cryogenic inducers are a necessary complement to experimental campaigns and are very useful in the early turbopump design stages. Simulations using RANS turbulence closure models provide detailed flow field characteristics, are computationally affordable, and can be integrated into optimization tools for rapid design convergence. At the same time, the uncertainty related to the flow modelling must be understood and quantified. This work highlights the non-negligible effect of the selection of the turbulence model on characteristic flow setups relevant to cryogenic turbopump inducers.

Many previous works [26, 34, 35] have highlighted the large influence of the choice of cavitation model. Yet the equally important effect of the turbulence model has, to the knowledge of the authors, not been systematically characterized in turbopump configurations. In this work, we showed that the choice of turbulence model plays an important role in the prediction of the cavitation size, and onset and, concomitantly, on the integral flow characteristics. The sensitivity of the choice of turbulence models depends primarily on two parameters: (1) the choice of cavitation solver; (2) the type of flow simulated.

The variation among the turbulence models is the greatest for cavitation solvers that directly couple the density and the pressure (barotropic models); transport equation solvers show far less variation among the turbulence models. The variability of cavitation predictions among the turbulence models also depends on the type of flow under consideration. In bounded flow problems, as occurring in blade passage cavitation in cryogenic turbopumps, the cavitation predictions by different RANS-based turbulence models varies drastically. This large uncertainty may lead to drastic variations in the predicted pump efficiency and for other important design parameters. In the case of non-bounded flows (or in which the bounding walls have a limited effect on cavitation), the results are, for the most part, insensitive to the choice of turbulence models (particularly for TES). Furthermore, rotation causes a strong deviation of the velocity profile from the logarithmic law, which results in the invalidation of standard wall functions for wall treatment [36].

Inclusion of source terms in turbulence models to account for multiphase interactions, rotational wall boundary conditions, and problem specific corrections to account for rotation flow anisotropies and flow unsteadiness can lead to an improvement in predictive capabilities of numerical simulations. Accurate predictive capabili-

ties are desired and in many cases required to save development costs. These extensions to classical should be considered as further research.

5 Acknowledgements

This work was carried out at the German Space Center (DLR) in the Spacecraft Department of the Institute of Aerodynamics and Flow Technology, in Göttingen, Germany in collaboration with Delft University of Technology, the Netherlands. The authors would like to thank Prof. Dr.-Ing. Klaus Hannemann, head of the Spacecraft Department in DLR and Dr. Eberhard Gill, the head of Space Systems Engineering in TU Delft.

References

[1] Sutton, G., and Bilbarz, O., 2010. *Rocket Propulsion Elements 7th Edition*. Wiley.

[2] Wu, Y., Li, S., Liu, S., Dou, H.-S., and Qian, Z., 2013. *Vibration of hydraulic machinery*. Springer.

[3] Stripling, L., and Acosta, A., 1962. "Cavitation in turbopumps - part 1". *Journal of Fluids Engineering,* **84**(3), pp. 326–338.

[4] Cervone, A., Torre, L., Pasini, A., and d'Agostino, L., 2009. "Cavitation and turbopump hydrodynamics research at alta spa and pisa university". In *Fluid Machinery and Fluid Mechanics*. Springer, pp. 80–88.

[5] Cervone, A., Testa, R., Bramanti, C., Rapposelli, E., and D'Agostino, L., 2005. "Thermal effects on cavitation instabilities in helical inducers". *Journal of Propulsion and Power,* **21**(5), pp. 893–899.

[6] Torre, L., Cervone, A., Pasini, A., and d'Agostino, L., 2011. "Experimental characterization of thermal cavitation effects on space rocket axial inducers". *Journal of Fluids Engineering,* **133**(11), p. 111303.

[7] d'Agostino, L., 2013. "Turbomachinery developments and cavitation". *VKI Lecture Series on Fluid Dynamics Associated to Launcher Developments, von Karman Institute of Fluid Dynamics, Rhode-Saint-Genese, Belgium, Apr*, pp. 15–17.

[8] Tsujimoto, Y., Yoshida, Y., Maekawa, Y., Watanabe, S., and Hashimoto, T., 1997. "Observations of oscillating cavitation of an inducer". *Journal of Fluids Engineering,* **119**(4), pp. 775–781.

[9] Kikuta, K., Yoshida, Y., Watanabe, M., Hashimoto, T., Nagaura, K., and Ohira, K., 2008. "Thermodynamic effect on cavitation performances and cavitation instabilities in an inducer". *Journal of Fluids Engineering,* **130**(11), p. 111302.

[10] Hickel, S., 2015. "Dns and les of two-phase flows with cavitation". In *Direct and Large-Eddy Simulation IX*. Springer, pp. 595–604.

[11] Pope, S. B., 2000. *Turbulent flows*. Cambridge university press.

[12] Payri, R., Tormos, B., Gimeno, J., and Bracho, G., 2010. "The potential of large eddy simulation (les) code for the modeling of flow in diesel injectors". *Mathematical and Computer Modelling,* **52**(7), pp. 1151–1160.

[13] Ahuja, V., Hosangadi, A., and Arunajatesan, S., 2001. "Simulations of cavitating flows using hybrid unstructured meshes". *Journal of Fluids Engineering,* **123**(2), pp. 331–340.

[14] Goncalvès, E., 2011. "Numerical study of unsteady turbulent cavitating flows". *European Journal of Mechanics-B/Fluids,* **30**(1), pp. 26–40.

[15] Decaix, J., and Goncalvès, E., 2012. "Time-dependent simulation of cavitating flow with k- turbulence models". *International Journal for Numerical Methods in Fluids,* **68**(8), pp. 1053–1072.

[16] Decaix, J., 2012. "Modlisation et simulation de la turbulence compressible en milieu diphasique: application aux coulements cavitants instationnaire". PhD thesis, University of Grenoble.

[17] Wu, J., Utturkar, Y., and Shyy, W., 2003. "Assessment of modeling strategies for cavitating flow around a hydrofoil". In Fifth International Symposium on Cavitation, Osaka, Japan, Nov, pp. 1–4.

[18] Wu, J., Wang, G., and Shyy, W., 2005. "Time-dependent turbulent cavitating flow computations with interfacial transport and filter-based models". *International Journal for Numerical Methods in Fluids,* **49**(7), pp. 739–761.

[19] Mashayek, F., and Pandya, R., 2003. "Analytical description of particle/droplet-laden turbulent flows". *Progress in Energy and Combustion science,* **29**(4), pp. 329–378.

[20] Cokljat, D., Slack, M., Vasquez, S., and Bakker, A., 2006. "Reynolds-stress model for eulerian multiphase". *Progress in Computational Fluid Dynamics,* **6**(1), pp. 168–178.

[21] Beishuizen, N., Naud, B., and Roekaerts, D., 2007. "Evaluation of a modified reynolds stress model for turbulent dispersed two-phase flows including two-way coupling". *Flow, Turbulence and Combustion,* **79**(3), pp. 321–341.

[22] Weller, H. G., Tabor, G., Jasak, H., and Fureby, C., 1998. "A tensorial approach to computational continuum mechanics using object-oriented techniques". *Computers in Physics,* **12**(6).

[23] Brennen, C. E., 2005. *Fundamentals of Multiphase Flow*. Cambridge University Press.

[24] Goncalvès, E., 2014. "Modeling for non isothermal cavitation using 4-equation models". *International Journal of Heat and Mass Transfer,* **76**, pp. 247–262.

[25] Kunz, R. F., Boger, D. A., Stinebring, D. R., Chyczewski, T. S., Lindau, J. W., Gibeling, H. J., Venkateswaran, S., and Govindan, T., 2000. "A preconditioned navier–stokes method for two-phase flows with application to cavitation prediction". *Computers & Fluids,* **29**(8), pp. 849–875.

[26] Senocak, I., and Shyy, W., 2002. "A pressure-based method for turbulent cavitating flow computations". *Journal of Computational Physics,* **176**, pp. 363–383.

[27] Wilcox, D. C., et al., 1998. *Turbulence modeling for CFD*, Vol. 2. DCW industries La Canada, CA.

[28] Mani, K., 2015. "Turbulence modelling of cavitating flows in cryogenic turbopumps". Master's thesis, Delft University of Technology.

[29] Rouse, H., and McNown, J. S., 1948. "Cavitation and pressure distribution: head forms at zero angle of yaw".

[30] Hord, J., 1973. *Cavitation in Liquid Cryogens: Hydrofoil. II*, Vol. 2156. National Aeronautics and Space Administration.

[31] Launder, B. E., and Spalding, D., 1974. "The numerical computation of turbulent flows". *Computer Methods in Applied Mechanics and Engineering,* **3**(2), pp. 269–289.

[32] Reboud, J., Coutier-Delgosha, O., Pouffary, B., and Fortes-Patella, R., 2003. "Numerical simulation of unsteady cavitation flows: Some applications and open problems". In Fifth International Symposium on Cavitation.

[33] Yakhot, V., Orszag, S., Thangam, S., Gatski, T., and Speziale, C., 1992. "Development of turbulence models for shear flows by a double expansion technique". *Physics of Fluids,* **4**(7), pp. 1510–1520.

[34] Utturkar, Y., Wu, J., Wang, G., and Shyy, W., 2005. "Recent progress in modeling of cryogenic cavitation for liquid rocket propulsion". *Progress in Aerospace Sciences,* **41**(7), pp. 558–608.

[35] Singhal, A. K., Athavale, M. M., Li, H., and Jiang, Y., 2002. "Mathematical basis and validation of the full cavitation model". *Journal of Fluids Engineering,* **124**(3), pp. 617–624.

[36] Jakirlic, S., Hanjalic, K., and Tropea, C., 2002. "Modeling rotating and swirling turbulent flows: a perpetual challenge". *AIAA Journal,* **40**(10), pp. 1984–1996.